

Electromechanical Properties and Charge Transport of $\text{Ca}_3\text{TaGa}_3\text{Si}_2\text{O}_{14}$ (CTGS) Single Crystals at Elevated Temperatures

Yuriy Suhak¹, Michal Schulz¹, Ward L. Johnson², Andrei Sotnikov³, Hagen Schmidt³,
Holger Fritze¹.

¹Clausthal University of Technology, Am Stollen 19B, Goslar, 38640, Germany.

²National Institute of Standards and Technology, 325 Broadway St., Boulder, CO 80305,
U.S.A.

³Leibniz Institute for Solid State and Materials Research Dresden, Helmholtzstr. 20, Dresden,
01069, Germany.

Abstract.

Structurally ordered piezoelectric $\text{Ca}_3\text{TaGa}_3\text{Si}_2\text{O}_{14}$ (CTGS) single crystals are studied. The elastic and piezoelectric constants are determined in the temperature range from 20 °C to 900 °C by two independent approaches: resonant and pulse-echo acoustic methods. Further, the temperature dependent acoustic losses are examined. These investigations reveal two loss peaks with maxima near 68 °C and 416 °C at 4.5 MHz that are attributed to anelastic point defect relaxations. Further, the transport of oxygen is investigated using the isotope ^{18}O as a tracer at temperatures from 1000 °C to 1200 °C. It is shown that the oxygen self-diffusion coefficients are at least three orders of magnitude lower than those of langasite, which is one reason for relatively low losses in CTGS at temperatures on the order of 1000 °C. Finally, the long-term stability of fundamental materials properties including electrical conductivity and resonance frequency is examined at 1000 °C. After one year of thermal treatment, the resonance frequency of resonators made from crystals of different sources is found to decrease only between 0.1 % and 0.4 %.

1. Introduction

The optimization of many technologies involving high temperatures requires improved

control systems and, therefore, sensors that can be operated in extreme environments. Thereby, the usage of piezoelectric materials as a sensing platform for high-temperature applications plays an important role in automotive, aerospace or energy industries due to the compactness, fast response and high sensitivity of such devices. Many of the traditional piezoelectric materials like α -quartz, lithium niobate or aluminum nitride face, however, restrictions on their high-temperature use, including instability, phase transformation, pyroelectricity, etc. [1,2,3,4].

Langasite (LGS, $\text{La}_3\text{Ga}_5\text{SiO}_{14}$) and its isomorphs attract increasing attention, since they do not exhibit phase transformations up to their melting points in the range from 1300 °C to 1500 °C [5,6]. Further, these crystals possess high piezoelectric coefficients, show piezoelectric response even at temperatures very close to the melting point [7,8,9], and can be rapidly grown in the form of large high-quality crystals by the Czochralski technique [9,10]. Generally, crystals in the langasite family can be divided into two types: disordered crystals, in which the same element occupies different cationic sites, and ordered crystals, in which each cationic site is occupied by a different element [6,11]. Ordered crystals show improved electromechanical properties, in particular, lower electrical conductivity and associated acoustic loss, resulting in greater resonance quality factors Q [6,12]. This issue is of practical relevance, since the quality factor must be maximized to improve the signal-to-noise ratio of a resonant sensor.

Catangasite (CTGS, $\text{Ca}_3\text{TaGa}_3\text{Si}_2\text{O}_{14}$) is a fully ordered compound of the langasite crystal family that was firstly synthesized in the late 1990s [13]. Its melting temperature is approximately 1370 °C. Previous investigations indicate significantly improved thermal stability of dielectric and piezoelectric properties compared to other crystals of the langasite family [12,14,15,16,17]. In order to evaluate the stability of CTGS in more detail, investigations and correlation of its electromechanical properties, such as piezoelectric, dielectric and elastic constants, electrical conductivity and acoustic losses, must be performed

as a function of temperature. Further, an understanding of the defect chemistry and transport mechanisms at high temperatures is required to evaluate the chemical stability of CTGS. Finally, the fundamental properties of CTGS over long periods of time must be investigated, since long-term stability is essential for industrial applications. To the best of our knowledge, a correlated investigation of CTGS electromechanical properties, defect chemistry and atomistic transport mechanisms at elevated temperatures has not yet been reported.

This work includes the determination of elastic and piezoelectric constants of CTGS from ambient temperature to 900 °C using two independent approaches: resonant and pulse-echo acoustic methods. Measurements and analysis of the full set of material constants presented here proceeds beyond our previous report of material constants [18] by considering thermal expansion of the material. The acoustic losses in CTGS are determined up to 900 °C and related to loss mechanisms. The analysis of transport kinetics in CTGS at high temperatures is performed by application of stable tracer isotope ^{18}O and subsequent secondary ion mass spectrometry to determine the oxygen self-diffusion coefficients and related ionic conductivity. Finally, the resonant properties and electrical conductivity of CTGS resonators are examined during one year of uninterrupted thermal treatment at 1000 °C in air, which enables an evaluation of long-term stability.

2. Sample preparation and experimental details

CTGS crystals used in this study are grown by the Czochralski technique. The mass density at room temperature, $\rho_{RT} = 4620 \text{ kg/m}^3$, used here is taken from the study of Sotnikov *et al.* [19], where its value was determined by the Archimedes method.

2.1. Material properties

Determination of the elastic and piezoelectric constants by the resonant method was performed on crystals provided by the Institute for Crystal Growth (IKZ), Berlin, Germany.

The crystal cut notation, required crystal cuts, and geometries match those of the IEEE standard [20]. Four rods with different orientation, namely (XYt)+0°, (XYt)+30°, (XYt)-30° and (XYt)-47°, and dimensions of 2×0.5×10 mm³ were operated in the length-extensional mode. A Y-cut plate with dimensions of 10×10×0.5 mm³ and a Y-cut disk with 10 mm diameter and 0.3 mm thickness are operated in a face-shear and a thickness-shear mode, respectively. The orientation accuracy was within 0.5°. The samples were coated with platinum electrodes by pulsed laser deposition (thickness ~ 300 nm). Subsequently, the resonators were placed in a tube furnace and heated to 900 °C. The resonance spectra were measured in air at atmospheric pressure and a heating rate of 1 K/min by a high-speed network analyzer (Agilent E5100A¹). Detailed description of the resonance method is given in [18,21].

The sound velocity was determined with a RITEC Advanced Ultrasonic Measurement System RAM-5000 on crystals manufactured by Fomos-Materials, Moscow, Russia. For this purpose, crystal cubes of 7×7×7 mm³ are prepared in two different orientations: (i) with the edges parallel to the main crystallographic axes X, Y, Z, and (ii) rotated by 45° around the X axis, so the edges are parallel to the (XYt)-45° and (XYt)+45° directions. The orientation accuracy was within 0.1°. The piezoelectric and elastic constants were then derived using a system of relations between sound velocities measured at characteristic directions for different modes (see, e.g, [22]). A more detailed description of the pulse-echo method can be found in previous publications [18,19].

The thermal expansion of the CTGS samples was determined using a Netzsch DIL-402E dilatometer. Two (XYt)+0° and (XZt)+0° CTGS rods with dimensions of 4x4x20 mm³ were prepared for this purpose.

¹ Certain trade names and company products are identified in this paper to adequately describe experimental methods. Such identification does not imply recommendation or endorsement by the National Institute of Standards and Technology, nor does it imply that the products are necessarily the best for the purpose.

The investigation of the electrical conductivity was performed by AC impedance spectroscopy in the frequency range from 1 Hz to 1 MHz using an impedance/gain-phase analyzer (Solartron 1260). An electrical equivalent-circuit model consisting of a constant phase element connected in parallel with a bulk resistance R_B was fitted to data. The bulk conductivity σ was then calculated through the relation $\sigma = t(AR_B)^{-1}$, where t and A are the thickness of the sample and the electrode area, respectively.

2.2. Acoustic losses

The investigations of acoustic losses were performed on Y-cut CTGS resonators, operated in the thickness-shear mode at the Clausthal University of Technology (TUC) by means of the impedance spectroscopy technique and at the National Institute of Standards and Technology (NIST) with a tone-burst excitation technique. [The oscillating electric field is applied along the Y-direction, which results in mechanical displacements in the X-direction. In other words, the disc undergoes a shearing through the thickness, which is described in more detail in \[23,24\].](#) Two resonators with a diameter of 14 mm and fundamental frequencies of 5.8 MHz and 4.5 MHz were manufactured from Fomos and IKZ single crystals, respectively, and denoted as Fomos-01 and IKZ-02, respectively.

Measurements at NIST were performed on the IKZ-02 specimen without electrode films at a total pressure less than 3×10^{-4} Pa above 100 °C and less than 25 Pa below 100 °C. Transduction was accomplished with noncontacting electrodes. The crystal holder, noncontacting electrodes, electronic system, and methods employed in these measurements are described elsewhere [25]. The specimen for measurements at TUC (Fomos-01) was coated with 3 μ m keyhole-shaped electrodes that were deposited by screen printing (print ink: Ferro Corporation, No. 6412 0410). Subsequently, the resonator was annealed at 1000 °C for about 30 min. The platinum-electroded sample was then mounted in an alumina holder inside a tube furnace and heated at a rate of 1 K/min. The electrical impedance of the sample was

examined in the vicinity of the resonance frequency by the high-speed network analyzer (Agilent E5100A). Fitting a Lorentz function to the resonant peaks of the real part of the admittance allows extracting the resonant frequency position and quality factor Q of the sample. This procedure is described in more detail by Schneider *et al.* [26].

2.3. Impurities

In order to better understand the processes that occur at elevated temperatures in the defect subsystem of the crystal, the impurity concentration in the investigated samples was determined by means of high-precision laser-ablation inductively coupled plasma mass spectrometry (LA-ICP-MS). This method is described in detail by Oeser *et al.* [27].

2.4. Diffusion experiments

Oxygen self-diffusion experiments were performed using the stable tracer isotope ^{18}O on CTGS samples manufactured by IKZ. The samples were placed in a furnace tube containing a gas atmosphere of 200 mbar that contained 95% $^{18}\text{O}_2$ and 5% $^{16}\text{O}_2$. Prior to each diffusion run, the samples were pre-annealed in air at the same temperatures and four times the duration of the diffusion run to ensure stable conditions. Table 1 summarizes annealing temperatures and times for different CTGS samples.

Table 1. Annealing temperatures and times for CTGS samples

Annealing Temperature	Pre-Annealing Time	$^{18}\text{O}_2$ -Annealing Time
1000 °C	192 h	48 h
1100 °C	96 h	24 h
1200 °C	48 h	12 h

Subsequently, the concentration depth profiles of the oxygen tracer were analyzed by secondary ion mass spectrometry (SIMS) using a Hiden Analytical SIMS system that employed an oxygen primary beam (5 keV, 200 nA). The sputtered area was $0.5 \times 0.5 \text{ mm}^2$, and the gating area was $0.1 \times 0.1 \text{ mm}^2$. The secondary ion intensities I of ^{18}O and ^{16}O were

measured as a function of time and converted to relative concentration $c(^{18}\text{O})$ of ^{18}O using the following expression:

$$c(^{18}\text{O}) = \frac{I(^{18}\text{O})}{I(^{16}\text{O}) + I(^{18}\text{O})} \cdot \quad (1)$$

2.5. Long-term stability

The long term stability of CTGS was examined by determining conductivity and resonance frequency of the samples at 1000°C in air. Bulk acoustic resonators (diameter 10 mm, thickness 300 μm) were manufactured from IKZ and SICCAS (Shanghai, China) crystals and used for this purpose. They are denoted by IKZ-L and SIC-L, respectively. The electrodes for the samples were prepared by the screen-printing technique.

3. Results and discussion

3.1. Impurities

Generally, the concentration of impurities in oxide crystals depends mostly on the growth conditions and starting materials. Table 2 shows the impurity concentrations in CTGS samples used in this study as determined by the LA-ICP-MS technique. Prior to these measurements, the mass spectra of the investigated samples were obtained by SIMS to identify the elements to be investigated by LA-ICP-MS.

Table 2. Determined impurities in investigated CTGS samples.

	Fomos-01 [ppm]	IKZ-02 [ppm]	SIC-L [ppm]	IKZ-L [ppm]
B	1.30±0.48	2.73±0.51	1.44±0.43	1.24±0.42
Cr	6.67±1.4	5.91±1.45	5.81±1.28	6.04±1.44
Ni	3.15±0.22	2.78±0.3	2.62±0.24	2.38±0.21
Zn	1.76±0.39	1.50±0.55	1.75±0.45	1.65±0.55
Ge	1.2±0.23	1.17±0.29	1.3±0.27	1.57±0.29
Sr	74.24±0.49	13.19±0.15	24.14±0.2	12.77±0.14
Y	0.15±0.018	0.07±0.016	3.17±0.057	0.07±0.018

Zr	0.44±0.08	0.17±0.06	16.32±0.36	0.16±0.06
Nb	0.22±0.02	1.18±0.04	0.24±0.02	1.16±0.03
Mo	<0.01	0.22±0.05	<0.01	0.24±0.06
Cd	77.98±1.44	78.13±1.51	79.56±1.29	77.72±1.39
Ba	1.64±0.10	1.16±0.11	1.51±0.09	1.2±0.10
La	36.65±0.22	0.41±0.021	32.35±0.29	0.41±0.018
Ce	0.07±0.01	0.11±0.008	0.05±0.006	0.10±0.008
Pr	<0.01	0.044±0.005	<0.01	0.045±0.005
Nd	<0.01	<0.01	<0.01	<0.01
Hf	6.38±0.19	6.52±0.22	7.03±0.19	6.39±0.20
W	10.11±0.27	10.18±0.31	10.00±0.30	9.97±0.32

As seen in Table 2, most detected elements show concentrations on the order of 2 ppm or less. Impurities such as Sr, Cd, Hf and W arise most probably from the starting materials, since Hf and W are commonly present at ppm levels in Ta₂O₅, and Cd and Sr are common impurities in SiO₂ and CaO, respectively. It should be noted that the samples show optical differences that presumably arise from differences in concentrations of impurities and/or intrinsic defects – the IKZ and Fomos crystals are completely transparent in visible spectral region, while the SICCAS crystal has yellowish color. Similar optical variations have been reported for other crystals in the langasite family [28].

The analysis also reveals somewhat greater concentrations of La in Fomos-01 and La, Zr and Y in SIC-L samples that are potentially connected with the growth conditions of the crystals. The influence of specific impurities on electromechanical and optical properties of CTGS samples was not in the scope of the current study. However, it should be noted that point defect concentrations even at ppm levels can introduce significant contributions to loss and conductivity [29].

3.2. Acoustic losses

The temperature dependent contributions to the acoustic losses in CTGS have previously been studied only in the work of Johnson *et al.* [25], where the losses in singly

rotated (YXt)-30° CTGS samples are compared to those of Y-cut CTGS, LGS and LGT (La₃Ga_{5.5}Ta_{0.5}O₁₄). In that work, the authors conclude that point-defect relaxations superimposed on contributions that increase monotonically with temperature are the greatest contributions to the material damping in the temperature range from ambient temperatures to 700 °C in (YXt)-30° and Y-cut CTGS samples. Above that temperature, the dominant physical mechanism remains unclear [25].

Based on the previous studies of acoustic losses in LGS, LGT and CTGS, the following physical mechanisms can contribute to the loss Q^{-1} [25,28]:

- (1) Losses connected with intrinsic phonon-phonon interactions. This contribution shows, however, a weak dependence above room temperature [30]. Since, overall, Q^{-1} in CTGS is found to increase strongly with temperature, the contribution of phonon-phonon losses becomes insignificant at elevated temperatures.
- (2) Losses caused by anelastic point defect relaxations. These losses are dependent on temperature and frequency, with the general form of a Debye function [29]:

$$Q^{-1}(\omega, T) = \frac{\Delta}{T} \frac{\omega\tau}{1 + \omega^2\tau^2}, \quad (2)$$

where Δ is a temperature-independent constant proportional to the concentration of relaxing defects, T is the absolute temperature, ω is the angular frequency (equal to $2\pi f$), τ is the relaxation time with an Arrhenius-like dependence on temperature,

$$\tau = \gamma \exp\left(\frac{E}{kT}\right), \quad (3)$$

γ is a time constant, E is the activation energy and k is Boltzmann's constant.

- (3) Temperature-dependent background that increases monotonically with increasing temperature. The physical source of this contribution has not been established. However, in [28] it is suggested that, in LGS and LGT, this contribution can arise

from anelasticity of growth-related structural defects. In [25] a similar physical loss mechanism is proposed for CTGS samples.

- (4) Losses connected with piezoelectric/carrier relaxation that contribute to Q^{-1} at elevated temperatures. This contribution can be approximated by a Debye function [28,31]:

$$Q_c^{-1}(\omega, T) \approx K^2 \frac{\omega \tau_c}{1 + \omega^2 \tau_c^2}, \quad (4)$$

where, K^2 and τ_c are the electromechanical coupling coefficient and the relaxation time, respectively, with $\tau_c = 1/(2\pi f_\varepsilon)$. The conductivity-related contribution has a maximum at the temperature where the dielectric relaxation frequency $f_\varepsilon = \sigma/2\pi\varepsilon$ is equal to the acoustic frequency [32]. Here, σ is the electrical conductivity and ε is the dielectric constant.

- (5) Temperature independent contribution that arises from mounting, electrical leads and, if present, electrodes [24].

In order to evaluate the impact of conductivity related losses in CTGS, the temperature dependence of conductivity has to be considered. This property is presented in Fig. 1 and compared with data previously reported for LGS [33].

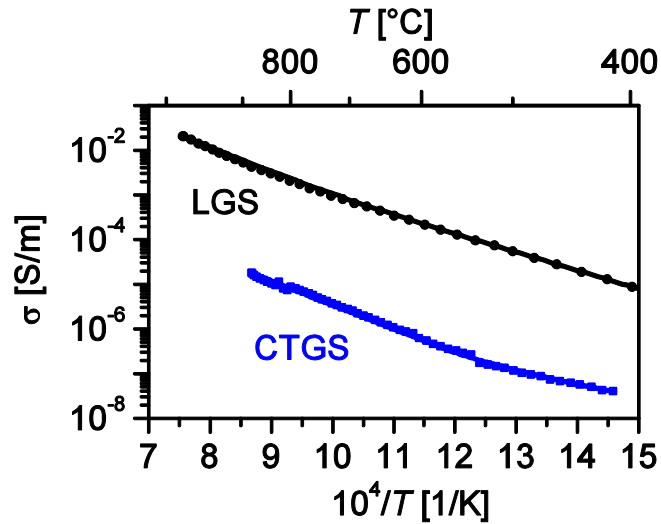


Figure 1. Temperature dependent electrical conductivity of CTGS and LGS.

As seen from Fig. 1, the conductivity of CTGS is at least two orders of magnitude lower than that of LGS over the entire measurement range. The data in Fig. 1 are used to calculate the corresponding dielectric relaxation frequencies plotted in Fig. 2. Resonators show strong conductivity-related losses at acoustic frequencies close to the dielectric relaxation frequency [32]. Thereby, the maximum of this loss contribution for LGS resonators operated at a fundamental frequency of about 5 MHz is found around 950 °C (Fig. 2) and equals $Q^{-1} = 1.5 \times 10^{-2}$ (Eq. 4). At 600 °C, this influence is significantly decreased and equals $Q^{-1} = 7.5 \times 10^{-4}$ which still impacts the overall loss. In contrast, the conductivity related losses of 5 MHz CTGS resonators are significantly lower, showing values of $Q^{-1} = 2 \times 10^{-4}$ and $Q^{-1} = 2 \times 10^{-6}$ at 950 °C and 600 °C, respectively. In conclusion, conductivity-related losses may affect CTGS resonators at sufficiently elevated temperatures. However, at 600 °C and below, conductivity related losses are significantly smaller than the measured total loss and, therefore, not considered in the following data evaluation up to about 600 °C for the fundamental mode at about 5 MHz. Similar arguments are valid for the third and fifth overtones, up to 650°C and 700°C respectively.

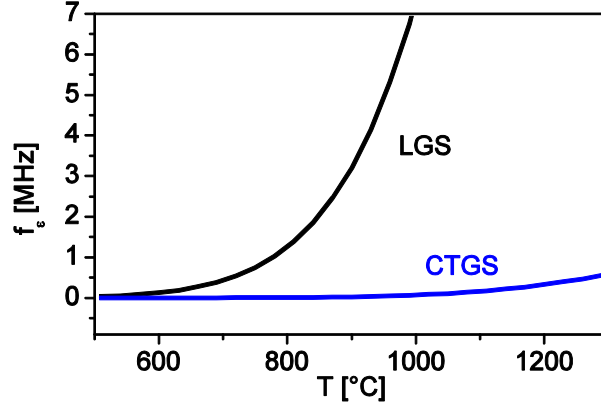


Figure 2. Dielectric relaxation frequency calculated using the electrical conductivity (see text for details) as a function of temperature for LGS and CTGS.

Fig. 3 presents a plot of temperature dependent Q^{-1} for the IKZ-02 CTGS sample, operated in the fundamental mode (4.5 MHz). Two peaks with maxima around 80 °C and 450 °C are visible. Similar peaks reported for singly rotated CTGS specimens were found to be consistent with anelastic point defect relaxations [25]. Considering the physical mechanisms described above, the following expression can be written to describe the overall losses Q^{-1} of CTGS resonators:

$$Q^{-1} = \frac{\Delta_1}{T} \frac{\omega\tau_1}{1 + \omega^2\tau_1^2} + \frac{\Delta_2}{T} \frac{\omega\tau_2}{1 + \omega^2\tau_2^2} + \Delta_3 \exp\left(\frac{-E_3}{kT}\right) + C_0, \quad (7)$$

where

$$\tau_1 = \gamma_1 \exp\left(\frac{E_1}{kT}\right), \quad \tau_2 = \gamma_2 \exp\left(\frac{E_2}{kT}\right). \quad (8)$$

The first and the second term of the expression (7) describe the contributions of anelastic point defects relaxations. The third term represents the temperature-dependent background that increases monotonically with temperature. The term C_0 describes the temperature

independent background. Expression (7) is fitted to the measured $Q^{-1}(T)$ values and visualized in Fig. 3 together with the separate contributions to Q^{-1} determined from the fit.

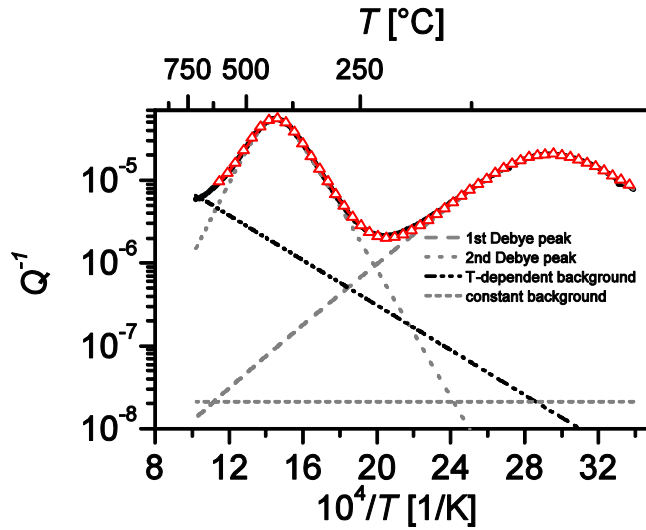


Figure 3. Measured $Q^{-1}(T)$ values for IKZ-02 CTGS sample, operated in the fundamental mode (solid line), corresponding fit (triangles) and separate fit contributions.

The $Q^{-1}(T)$ measurements of the third and fifth overtones of the IKZ-02 sample are presented in Fig. 4 and compared with the fundamental mode. The maximum of the Debye peaks shifts with increasing overtone number or frequency. At the highest measured temperatures (above ~ 830 °C), a loss increase is observed with increasing temperature for the third and fifth overtones. Measurements of the fundamental mode did not extend into this range, because of interference from one or more spurious modes. The increase of the loss of the higher overtones can be interpreted as part of another peak. The nature of this peak is expected to be investigated in a subsequent paper. Therefore, the fitting procedure to the expression (7) was applied up to the 600 °C, 650 °C and 700 °C for the fundamental mode, third and fifth overtones of the IKZ-02, respectively, in order to exclude possible influences of the high-temperature peaks on the fitting parameters.

The measurements of Q^{-1} of sample Fomos-01, operated in the fundamental mode at 5.8 MHz, are also plotted in Fig. 4. The minimum temperature for these measurements is

200 °C, therefore the first Debye peak is not observed. Accordingly, expression (7) is modified by setting $\Delta_1 = 0$.

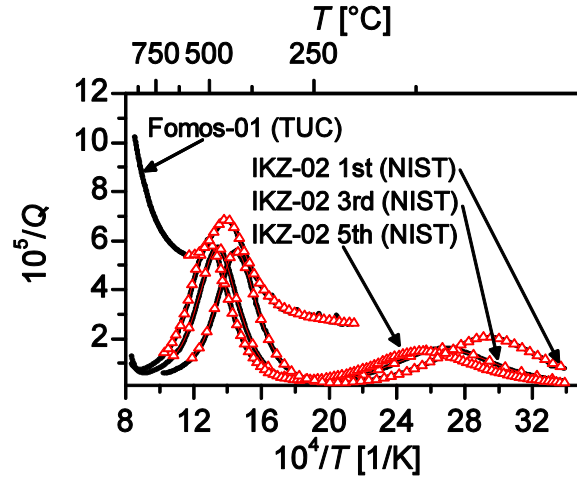


Figure 4. Measured $Q^{-1}(T)$ values (solid lines) and corresponding fits (triangles) for IKZ-02 and Fomos-01 samples.

The fitting of the expression (7) to the measured Q^{-1} data for the sample Fomos-01 is performed up to 600 °C. The fit parameters are summarized in Table 3.

Table 3. Fit parameters obtained for the $Q^{-1}(T)$ dependences for different samples.

	Fomos-01 fundamental mode	IKZ-02 fundamental mode	IKZ-02 3 rd overtone	IKZ-02 5 th overtone
f	5.8 MHz	4.5 MHz	13.4 MHz	22.4 MHz
Δ_1	–	1.40×10^{-2}	1.20×10^{-2}	1.16×10^{-2}
γ_1	–	7.78×10^{-13} s	7.91×10^{-13} s	5.84×10^{-13} s
E_1	–	0.32 eV	0.31 eV	0.31 eV
Δ_2	4.40×10^{-2}	7.42×10^{-2}	8.30×10^{-2}	8.75×10^{-2}
γ_2	2.08×10^{-14} s	4.58×10^{-14} s	4.08×10^{-14} s	2.41×10^{-14} s
E_2	0.86 eV	0.81 eV	0.81 eV	0.81 eV
Δ_3	5.06×10^{-4}	2.49×10^{-4}	3.32×10^{-4}	2.0×10^{-4}
E_3	0.22 eV	0.30 eV	0.33 eV	0.29 eV
C_0	2.42×10^{-5}	2.09×10^{-8}	1.73×10^{-8}	2.02×10^{-8}

The obtained values for the Debye peaks are typical for point defect relaxations [29].

Some minor deviations of the values for different overtones of IKZ-02 sample could be

connected with either the fit uncertainty or inaccuracy of the functional forms, such as the assumed frequency independence of C_0 and Δ_3 . The differences in fit parameters between Fomos-01 and IKZ-02 samples can be attributed predominantly to the presence of thick-film electrodes. In particular, note that the constant term C_0 for the contactless method (IKZ-02) is much smaller, indicating that the electrodes and the supporting structure employed in the Fomos-01 measurements contributed substantially to the overall losses. In addition, differences in crystal quality might contribute to measured differences in Q^{-1} of the two samples.

3.3. Transport kinetics at elevated temperatures

Oxygen is suspected to be the most mobile ion in CTGS. This suspicion is based on diffusion data for LGS, where the cations move significantly slower than oxygen at a given temperature [34]. The oxygen diffusion analysis in CTGS is performed using an analytical solution of Fick's second law [35]:

$$\frac{c - c_s}{c_0 - c_s} = \operatorname{erf}\left(\frac{x}{2\sqrt{Dt}}\right), \quad (9)$$

where c_s and c_0 are the concentration at the surface and the background concentration prior to the diffusion run, respectively. The distance from the surface is denoted by x . D and t are the diffusion coefficient and the annealing time, respectively. The relative ^{18}O concentration depth profiles are normalized according to Eq. 1. Subsequently, expression (9) is fitted to the data by varying the fitting parameters. That allows extracting the diffusion coefficients of ^{18}O ions, which are presented as a function of temperature in the Arrhenius plot in Fig. 5 and compared to those previously reported for LGS [36].

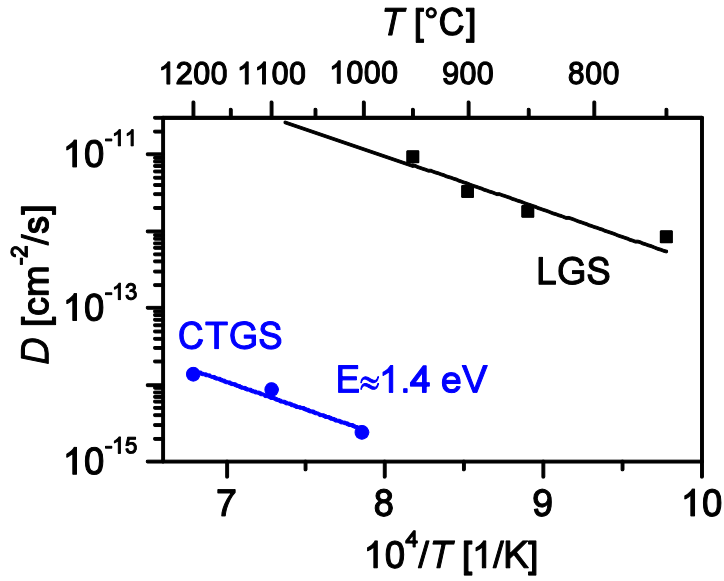


Figure 5. Oxygen diffusion coefficients obtained here for CTGS (circles) and previously obtained for LGS (squares) [36].

As seen from Fig. 5, the ^{18}O diffusion coefficients of LGS were obtained only up to 950 °C, so that the temperature ranges of the two data sets do not overlap. However, extrapolation of these data to higher temperatures allows one to conclude that the oxygen diffusion coefficient of CTGS is at least three orders of magnitude lower than that of LGS. This difference is approximately an order of magnitude greater than the difference in electrical conductivity of these materials (Fig. 1), [indicating that different mechanisms are responsible for the conductivity at sufficiently elevated temperatures \(see below\)](#). Using the expression:

$$D = D_0 \exp\left(\frac{-E}{kT}\right), \quad (10)$$

where D_0 and E are the pre-exponential coefficient and the activation energy of the oxygen diffusion process, respectively, the activation energy determined from a fit of the Arrhenius plot (Fig. 5) is $E \approx (1.4 \pm 0.2)$ eV. A similar activation energy of 1.4 eV for ^{18}O diffusion was

previously reported for LGS [36], though current estimation for CTGS appears to be rough and requires data in a larger temperature range for its more precise determination.

The determined coefficients of oxygen diffusion enable a calculation of the contribution of ionic conductivity from oxygen transport to the overall conductivity at a given temperature, using the expression [24,37]:

$$\sigma_o = \frac{(2q)^2}{kT} [O_o] D, \quad (11)$$

where $2q$ and $[O_o]$ are the charge of the mobile species and the oxygen concentration, respectively. At 1000 °C, σ_o is found to be $(3.8 \pm 0.6) \times 10^{-9}$ S/m, and this corresponds to only about 80 ppm of the overall conductivity. In other words, electronic conductivity dominates. Therefore, the conductivity mechanisms in CTGS at elevated temperatures differ from those in LGS, where ionic conduction is reported to be dominant at temperatures above 700 °C [33]

3.4. Elastic and piezoelectric constants

Correct determination of the elastic and piezoelectric constants at different temperatures requires compensation for thermal expansion of the material. Measurements of thermal expansion of the CTGS samples presented in Fig. 6 are used to calculate the temperature dependent density and dimensions of CTGS samples. It should be noted that, according to the crystal symmetry, the crystal expands with increasing temperature equally in the X- and Y- directions. Therefore, only the expansion in the Y-direction is plotted. As seen from Fig. 6, the expansion in this direction increases almost linearly over the entire measured temperature range. Greater deviations from linearity are observed in the Z-direction, especially at temperatures below 500 °C.

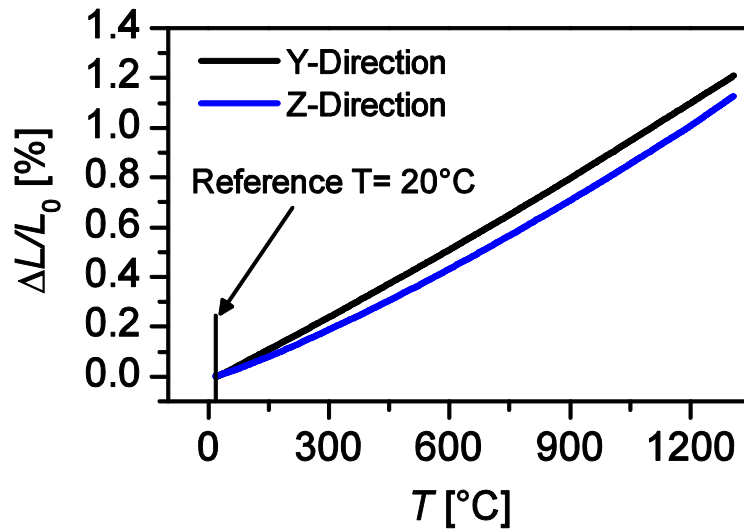


Figure 6. Thermal expansion of CTGS in different directions as a function of temperature.

Fig. 7 presents measurements of the temperature dependence of elastic stiffness constants C_{ij} , determined by the pulse-echo and resonant methods up to 800 °C and 900 °C, respectively (see Section 2.1). The temperature dependence of the elastic constants determined by the two methods is similar, with the exception of C_{13} and C_{33} . All the constants determined by the resonance method, except for the C_{44} , are found to decrease with increasing temperature.

Some divergence is observed for the absolute values of the constants. The values of C_{11} , C_{14} and C_{66} differ up to about 7.5 % in the whole measured temperature range. The elastic constant C_{33} shows a difference of about 3.3 %, 1.5 % and 8 % at room temperature, 400 °C and 800 °C respectively. According to our calculations, the uncertainty for C_{33} determination is below 8 % in the case of the resonance measurements. The uncertainties for C_{11} , C_{14} , and C_{66} are below 6 %, 5.5 % and 2 %, respectively. **It is necessary to note that the resonant method does not allow direct determination of C_{ij} stiffness constants except for C_{66} , which is extracted directly from the frequency characteristics of the thickness-shear mode**

resonator. The elastic compliance constants S_{ij} are determined instead and then used to calculate the C_{ij} . Thereby, the uncertainties for C_{ij} , are caused by accumulation of uncertainties for S_{ij} .

The absolute values of the elastic constants C_{44} , C_{12} and C_{13} , determined by the two methods, show somewhat greater differences. Values of C_{12} and C_{13} reported by other authors [16,17,38] show even greater variations (more than 35 % and 50 %, respectively, at room temperature). Sources of uncertainty in the determination of these constants (or actual physical variations in the constants) are unclear and require further investigations.

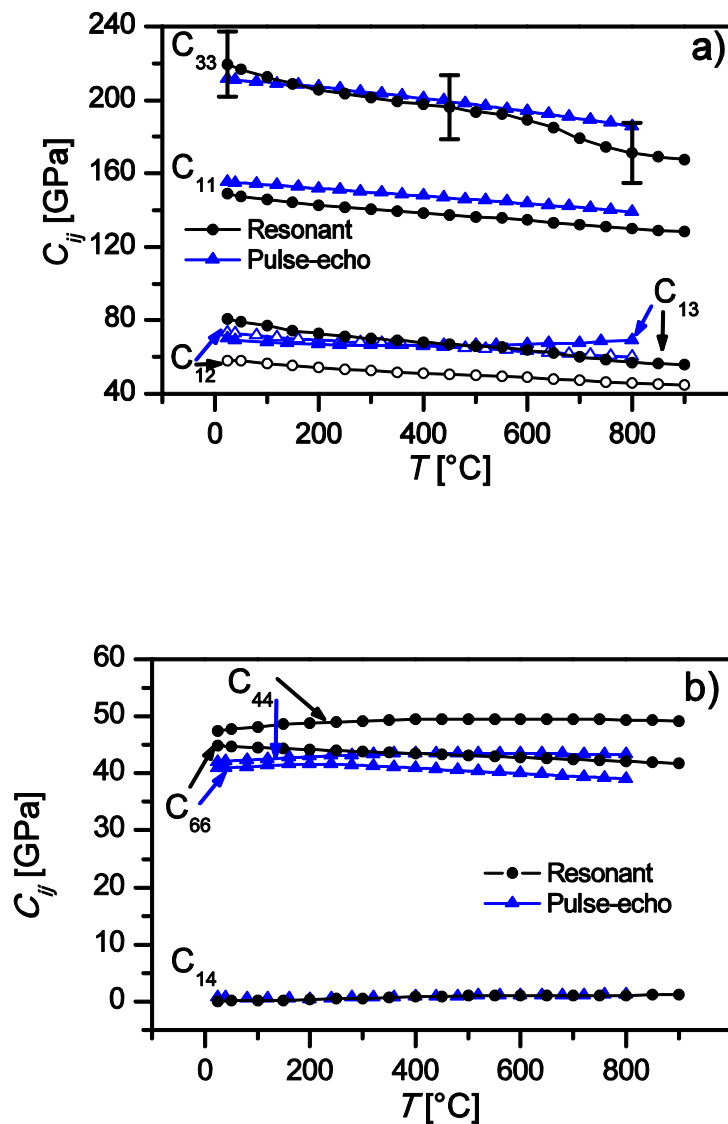


Figure 7. Elastic stiffness constants C_{ij} as a function of temperature: a) elastic constants C_{11} , C_{12} (open symbols), C_{13} , C_{33} ; b) elastic constants C_{14} , C_{44} , C_{66} . (Lines are for guiding the eyes only).

The temperature dependence of measured piezoelectric constants e_{11} and e_{14} is shown in Fig. 8. The values of piezoelectric constants determined by the resonant method are lower (by 8 % to 16 %) than those determined by the pulse-echo technique. The calculated uncertainty for e_{11} and e_{14} determined by the resonant method is about 8 %, which might explain the differences in e_{11} determined by the two methods. The differences in e_{14} require further investigations.

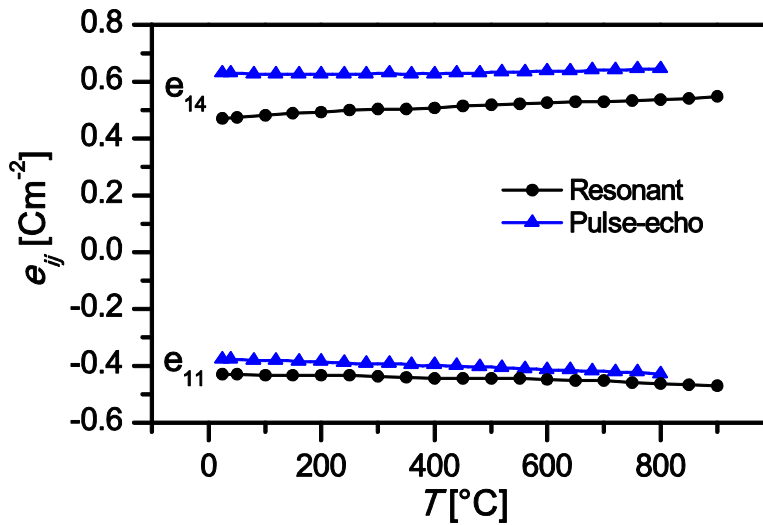


Figure 8. Piezoelectric constants e_{11} and e_{14} as a function of temperature. (Lines are for guiding the eyes only).

In order to validate the results of the resonant method, a physical model, described in Ref. [32], is fitted to measured resonance spectra of the Y-cut thickness-shear resonator. Among other parameters, this model enables an extraction of the elastic constant C_{66} and the piezoelectric constants $e_{26} = -e_{11}$. Fig. 9 presents the constants as obtained from analysis with

this model and from the resonance method. The results are in satisfactory agreement, with maximal differences of 0.5 % and 2 % in C_{66} and e_{11} , respectively. The uncertainty for C_{66} determined by the resonant method is also shown in Fig. 9.

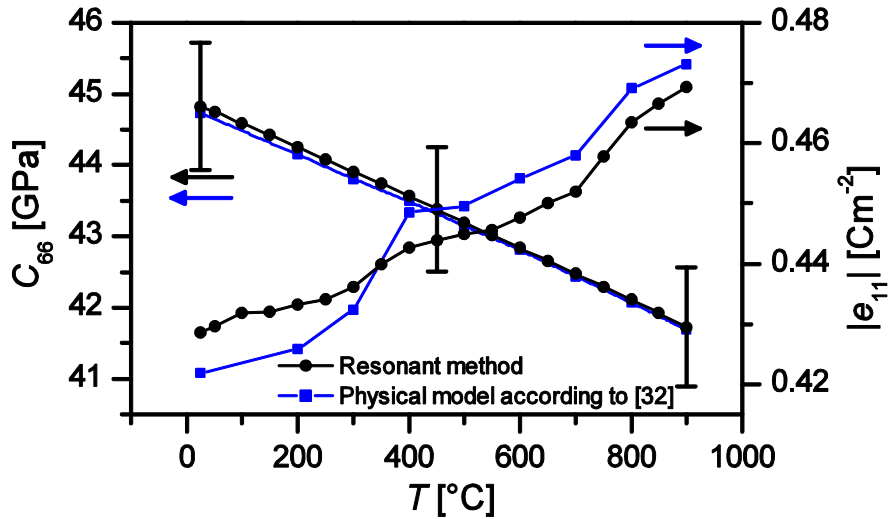


Figure 9. Temperature-dependent elastic constant C_{66} and piezoelectric constant e_{11} determined by the resonant method and through fitting spectra to the physical model [32]. (Lines are for guiding the eyes only).

3.5. Long-term properties

Evaluation of the operational limits of CTGS resonators requires investigation of their properties in harsh environments over long time periods. Therefore, the electrical conductivity and the resonance frequency of different CTGS specimens were examined at 1000 °C in air during one year of uninterrupted thermal treatment. We have reported the long-term properties of CTGS previously in [39]. In the current work, however, the duration of investigation is substantially increased. Further, the temperature control is improved. The time dependent electrical conductivities of different CTGS specimens are shown in Fig. 10. The initial conductivities are $(2.6 \pm 0.2) \times 10^{-5}$ S/m and $(3.1 \pm 0.2) \times 10^{-4}$ S/m for samples IKZ-L and SIC-L, respectively. However, within approximately 500 h of thermal treatment, the electrical

conductivity of IKZ-L increases and reaches a value of $(1.65 \pm 0.1) \times 10^{-4}$ S/m. SIC-L also shows an increase in conductivity. The changes of this sample are slower, reaching a value of $(5.3 \pm 0.3) \times 10^{-4}$ S/m after 1000 hours. The same general behavior was observed in our previous study [39]. Its origin remains unclear and will be investigated in terms of structural changes of crystals and electrodes.

After this initial period of time, the conductivity of all specimens remains nearly constant over the next 1500 hours of thermal treatment. In the period of 2000 h to 8600 h, the conductivity of IKZ-L shows some drift of about $\pm 10\%$, and that of SIC-L constantly decreases within the period of 2000-5200 h. After 5200 hours, the conductivity of SIC-L drops abruptly and after about 7500 h the signal is completely lost which is potentially caused by the degradation of electrodes. Presently, this hypothesis cannot be proved, since the experiment is still running with all samples.

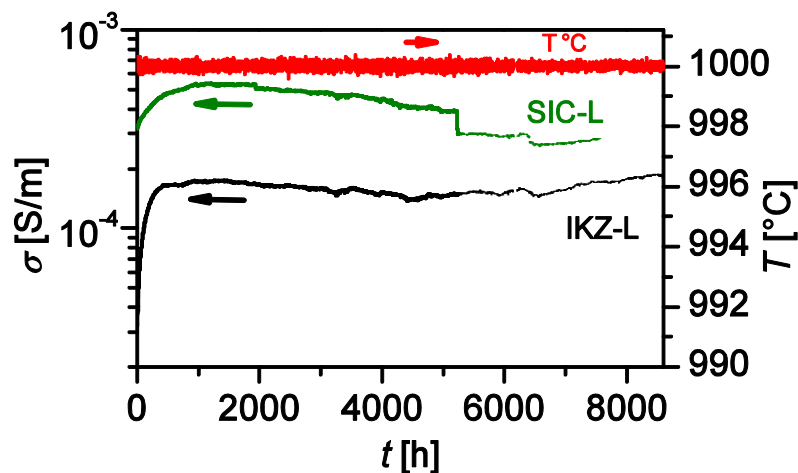


Figure 10. Time dependent electrical conductivity of different CTGS samples.

Fig. 11 shows the change of the fundamental resonance frequency of IKZ-L and SIC-L specimens as a function of time during annealing at 1000 °C, relative to initial values measured when 1000 °C was reached (f_0). A frequency shift is observed for the IKZ resonator during the first 500 hours of investigation. This shift occurs in the same time period as the initial relatively rapid changes in conductivity (see Fig. 10). Here, a physical correlation is suspected and must be investigated in concert with the defect chemical models. After this initial period, the resonance frequency steadily decreases, reaching a total shift of 0.4 % at 8500 h, relative to f_0 . A similar decrease is observed for the SIC-L specimen. Its behavior is more stable, showing a relative shift of only 0.1 % at 7500 h. Since the investigation of conductivity (Fig. 10) and resonance frequency is performed simultaneously on the same specimens, measurements of the frequency of SIC-L also ended at 7500 h.

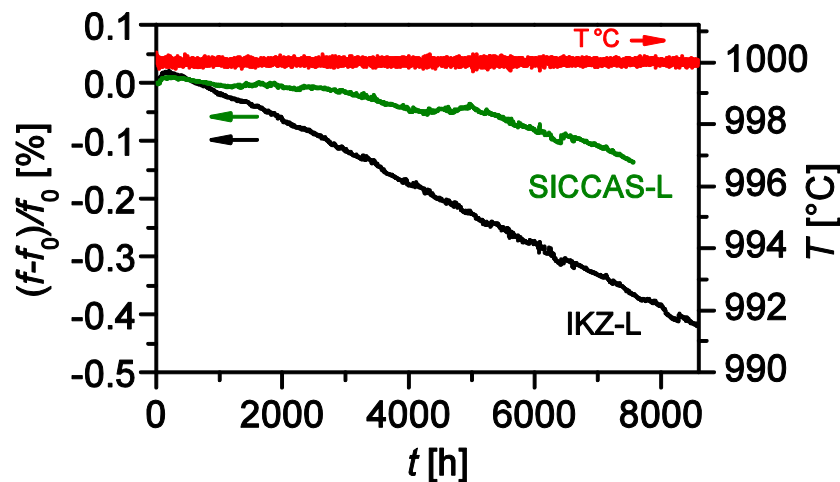


Figure 11. Time-dependent relative change of the resonance frequency of different CTGS samples.

4. Conclusions

In summary, various properties of CTGS are investigated at elevated temperatures. The measurement of temperature-dependent Q^{-1} revealed two peaks, and these peaks are attributed to anelastic point defect relaxations superimposed on a monotonically increasing temperature-dependent background and a constant contribution. Evidence of another contribution to acoustic loss was revealed at sufficiently elevated temperatures by the examination of the 3rd and 5th overtones of CTGS. The temperature-independent contribution to Q^{-1} that is not related to the crystal, appears to be much smaller for the contactless measurements, indicating that the electrodes and associated mechanical contact contribute to the overall losses significantly with contacting electrodes.

The investigations of transport mechanisms at elevated temperatures have led to the conclusion that the coefficients of oxygen diffusion in CTGS are at least three orders of magnitude lower than those of LGS. The contribution of ionic conductivity to the overall conductivity in CTGS at 1000 °C is found to be relatively small, indicating predominant electronic conduction.

The elastic and piezoelectric constants, determined by two independent methods, show similar temperature dependence. Observed differences in absolute values obtained with the two methods are a subject for subsequent research.

The investigation of CTGS long-term behavior reveals that the IKZ resonator shows piezoelectric response at least after one year of constant uninterrupted treatment at 1000 °C in air. The resonance frequency shows a relative shift of only 0.4 % during this period.

Acknowledgements. Research grants from the German Research Foundation (DFG: FR 1301/21-1 and SO 1085/2-1) made this work possible. Further, the support from the Energie-Forschungszentrum Niedersachsen is acknowledged. This paper is a contribution of the National Institute of Standards and Technology and not subject to copyright in the United States.

Literature.

- [1]. J. Haines, O. Cambon, D. Keen, M. Tucker and M. Dove, Structural disorder and loss of piezoelectric properties in α -quartz at high temperature, *Appl. Phys. Lett.*, **81** 2968-2970 (2002).
- [2]. R. Behanan, S. Moulzolf, M. Call, G. Bernhardt, D. Frankel, R. Lad and M. da Cunha, Thin films and techniques for SAW sensor operation above 1000 °C, *2015 Joint UFFC, EFTF and FM Symp.*, 1013–1016 (2015).
- [3]. D. Damjanovic, Materials for high-temperature piezoelectric transducers, *Curr. Opin. Solid St. M.* **3** 469-473 (1998).
- [4]. D. P. Birnie III, Analysis of diffusion in lithium niobate, *J. Mat. Sci.* **28** 302-315 (1993).
- [5]. J.A. Thiele and M. Pereira da Cunha, High temperature LGS SAW gas sensor, *Sens. Actuators B*, **22** 12002 (2011)
- [6]. H. Ohsato, T. Iwataki and H. Morikoshi, Crystal structure and piezoelectric properties of four component langasite $A_3BGa_3Si_2O_{14}$ ($A = Ca$ or Sr , $B = Ta$ or Nb), *Trans. Electr. Electron. Mater.* **13** 171-176 (2012).
- [7]. H. Fritze, H. L. Tuller, G. Borchardt and T. Fukuda, High-Temperature Properties of Langasite, *MRS Proceedings*, **604** 65-73 (1999).
- [8]. H. Fritze and H. L. Tuller, "U.S. Patent No. 6 370 955," 2002
- [9]. K. Shimamura, H. Takeda, T. Kohno and T. Fukuda, Growth and characterization of lanthanum gallium silicate $La_3Ga_5SiO_{14}$ single crystals for piezoelectric applications, *J. Cryst. Growth*, **163** 388–392 (1996).
- [10]. J. Bohm, R.B. Heimann, M. Hengst, R. Roewer and J. Schindler, Czochralski growth and characterization of piezoelectric single crystals with langasite structure: $La_3Ga_5SiO_{14}$ (LGS), $La_3Ga_{5.5}Nb_{0.5}O_{14}$ (LGN), and $La_3Ga_{5.5}Ta_{0.5}O_{14}$ (LGT) Part I, *J. Cryst. Growth*, **204** 128–136 (1999).

-
- [11]. X. Fu, E. G. Villora, Yo. Matsushita, Yu. Kitanaka, Yu. Noguchi, M. Miyayama, K. Shimamura and N. Ohashi, Influence of growth conditions on the optical, electrical resistivity and piezoelectric properties of $\text{Ca}_3\text{TaGa}_3\text{Si}_2\text{O}_{14}$ single crystals, *J. Ceram. Soc. Jpn.*, **124** 523-527 (2016).
- [12]. S. Zhang, Y. Zheng, H. Kong, J. Xin, E. Frantz and T.R. ShROUT, Characterization of high temperature piezoelectric crystals with an ordered langasite structure, *J. Appl. Phys.*, **105** 114107 (2009).
- [13]. B.V Mill, E.L.Belokoneva and T. Fukuda, New compounds with a $\text{Ca}_3\text{Ga}_2\text{Ge}_2\text{O}_{14}$ -type structure: $\text{A}(3)\text{XY}(3)\text{Z}(2)\text{O}(14)$ ($\text{A} = \text{Ca, Sr, Ba, Pb}$; $\text{X} = \text{Sb, Nb, Ta}$; $\text{Y} = \text{Ga, Al, Fe, In}$; $\text{Z} = \text{Si, Ge}$), *Russ. J. Inorg. Chem.*, **43** 1168-1175 (1998).
- [14]. F. Yu, Sh. Zhang, X. Zhao, D. Yuan, L. Qin, Q.-M. Wang and T.R. ShROUT, Investigation of $\text{Ca}_3\text{TaGa}_3\text{Si}_2\text{O}_{14}$ piezoelectric crystals for high temperature sensors, *J. Appl. Phys.*, **109** 114103 (2011).
- [15]. D. Roshchupkin, L. Ortega, O. Plotitsyna, A. Erko, I. Zizak, D. Irzhak, R. Fahrtdinov and O. Buzanov, Advanced piezoelectric crystal $\text{Ca}_3\text{TaGa}_3\text{Si}_2\text{O}_{14}$: growth, crystal structure perfection, and acoustic properties, *Appl. Phys. A*, **114** 1105-1112 (2014).
- [16]. X. Shi, D. Yuan, X. Yin, A. Wei, Sh. Guo and F. Yu, Crystal growth and dielectric, piezoelectric and elastic properties of $\text{Ca}_3\text{TaGa}_3\text{Si}_2\text{O}_{14}$ single crystal, *Solid State Commun.*, **142** 173–176 (2007).
- [17]. H. Zu, Q. Lin, H. Wu, Y. Zheng and Q.-M. Wang, Characterization of the dielectric, piezoelectric and elastic coefficients of $\text{Ca}_3\text{TaGa}_3\text{Si}_2\text{O}_{14}$ single crystals up to 800 °C, *IEEE Trans. Ultrason., Ferroelect., Freq. Control.* (2016) DOI 10.1109/TUFFC.2016.2544662.
- [18]. Yu. Suhak, M. Schulz, A. Sotnikov, H. Schmidt, S. Ganschow, S. Sakharov, H. Fritze, *Integr. Ferroelectr.*, Dielectric, piezoelectric and elastic constants of $\text{Ca}_3\text{TaGa}_3\text{Si}_2\text{O}_{14}$ single crystals at elevated temperatures, in press.

-
- [19] A. Sotnikov, H. Schmidt, M. Weihnacht, O. Buzanov and S. Sakharov, Material parameters of $\text{Ca}_3\text{TaGa}_3\text{Si}_2\text{O}_{14}$ single crystal revisited, *IEEE Int. Ultrason., Symp.*, 1688-1691 (2013).
- [20]. IEEE Standard on Piezoelectricity. *ANSI/IEEE Standards* **176** 1-66 (1987).
- [21]. M. Schulz and H. Fritze, Electromechanical properties of langasite resonators at elevated temperatures, *Renewable Energy* **33** 336-341 (2008).
- [22]. J.A. Kosinski, R.A. Pastore, E. Bigler, M. Pereira da Cunha, D.C. Malocha and J. Detaint, A review of langasite material constants from BAW and SAW data: toward an improved data set, *Proc. IEEE Int. Freq. Contr. Symp.*, 278-286 (2001).
- [23]. [A. Arnau Vives, Piezoelectric Transducers and Applications. Berlin: Springer, 2008.](#)
- [24]. H. Fritze, High temperature piezoelectric crystals and devices, *J. Electroceram.*, **26** 122-161 (2011).
- [25]. W. L. Johnson, M. Schulz, H. Fritze, High-temperature electroacoustic characterization of Y-cut and singly-rotated $\text{Ca}_3\text{TaGa}_3\text{Si}_2\text{O}_{14}$ resonators *IEEE Trans. Ultrason., Ferroelect., Freq. Control.* **61** 1433-1441 (2014).
- [26]. T. Schneider, D. Richter, S. Doerner, H. Fritze, P. Hauptmann, Novel impedance interface for resonant high-temperature gas sensors, *Sens. Actuators B* **111** 187 (2005).
- [27]. M. Oeser, S. Weyer, I. Horn and S. Schuth, High-Precision Fe and Mg Isotope Ratios of Silicate Reference Glasses Determined In Situ by Femtosecond LA-MC-ICP-MS and by Solution Nebulisation MC-ICP-MS, *Geostandards and Geoanalytical Research*, **38** 311-328 (2014).
- [28] W.L. Johnson, S.A. Kim, S. Uda and C.F. Rivenbark, Contributions to anelasticity in langasite and langatate, *J. Appl. Phys.*, **110** 123528-12 (2011).
- [29]. A.S. Nowick and B.S. Berry, Anelastic relaxation in crystalline solids. New York: Academic Press, 1972.

-
- [30]. W.P. Mason, Physical acoustics, principles and methods. New York: Academic Press, 1965.
- [31]. A. R. Hutson and D. L. White, Elastic wave propagation in piezoelectric semiconductors, *J. Appl. Phys.*, **33** 40–47 (1962).
- [32]. H. Fritze, High-temperature bulk acoustic wave sensors, *Meas. Sci. Technol.*, **22** 12002 (2011).
- [33]. H. Fritze, High temperature piezoelectric materials: Defect chemistry and electromechanical properties, *J. Electroceram.*, **17** 625-630 (2006).
- [34] M. Schulz, H. Fritze, H. L. Tuller and H. Seh, Diffusion-Related Implications for Langasite Resonator Operation, *IEEE Trans. Ultrason., Ferroelect., Freq. Control.*, **51** 1381-1387 (2004).
- [35]. J. Crank, The mathematics of diffusion, Clarendon Press, Oxford, 1975.
- [36]. J. Sauerwald, D. Richter, E. Ansorge, B. Schmidt and H. Fritze, Langasite based miniaturized functional structures: Preparation, high-temperature properties and applications, *Phys. Stat. Sol. A*, **208** 390-403 (2011).
- [37] . P.G. Shewmon, Diffusion in Solids, McGraw-Hill, New York, 1963.
- [38]. S. Biryukov, H. Schmidt, A. Sotnikov, M. Weihnacht, S. Sakharov and O. Buzanov, CTGS Material Parameters Obtained by Versatile SAW Measurements, *IEEE Int. Ultrason., Symp.*, 882-885 (2014).
- [39]. Yu. Suhak, M. Schulz, H. Wulfmeier, W. L. Johnson, A. Sotnikov, H. Schmidt, S.Ganschow, D. Klimm and H. Fritze, Langasite-Type Resonant Sensors for Harsh Environments, *MRS Advances*, **1** 1513-1518 (2016).